RESEARCH ARTICLE

Key Points:
- Influence of sudden stratospheric warming (SSW) on the ionosphere over Brazilian sector is investigated
- Observation of significant increase in VTEC and strong CEJ during SSW events of 2014
- Minor ionospheric irregularity occurrence is observed during SSW days compared to non-SSW days

Correspondence to:
R. de Jesus,
jesus.rodolfo@hotmail.com

An Investigation of the Ionospheric Disturbances Due to the 2014 Sudden Stratospheric Warming Events Over Brazilian Sector

R. de Jesus[1] [ID], I. S. Batista[1] [ID], O. F. Jonah[1,2], A. J. de Abreu[3], P. R. Fagundes[4], K. Venkatesh[4] [ID], and C. M. Denardini[1]

[1]Instituto Nacional de Pesquisas Espaciais, São José dos Campos, Brazil, [2]Massachusetts Institute of Technology, Haystack Observatory, Westford, MA, USA, [3]Instituto Tecnológico de Aeronáutica, Divisão de Ciências Fundamentais, São José dos Campos, Brazil, [4]Universidade do Vale do Paraíba/IP&D, São José dos Campos, Brazil

Abstract The present study investigates the ionospheric *F* region response in the Brazilian sector due to sudden stratospheric warming (SSW) events of 2014. The data used for this work are obtained from GPS receivers and magnetometer measurements during day of year (DOY) 01 to 120, 2014 at different stations in the equatorial and low-latitude regions in the Brazilian sector. In addition, the data obtained from Communication/Navigation Outage Forecasting System satellites during DOY 01 to 75 of 2014 are used. The main novelty of this research is that, during the 2014 SSW events, daytime vertical total electron content (VTEC) shows a strong increase on the order of about 23% and 11% over the equatorial and low-latitude regions, respectively. We also observed that the nighttime VTEC (SSW days) is increased by 8% and 33% over equatorial and low-latitude regions, respectively. The magnetometer measurements show a strong counterelectrojet during the SSW days. The results show an amplification of the 0.5 day and ~2–16 day periods in the VTEC and equatorial electrojet during the SSWs. The occurrences of ionospheric irregularities during the SSW events are around 84% and 53% in the equatorial and low-latitude regions, respectively, which is less frequent when compared with those during the pre-SSW periods.

1. Introduction

Interaction between the stratospheric and ionospheric regions is a challenging problem to the scientific community (Bessarab et al., 2012). In the past few years, several investigations have focused on understanding the connection between ionospheric variability and changes in the lower atmosphere during the sudden stratospheric warming (SSW) events (Fang et al., 2012, 2014). However, the detailed physical processes involved in the connection between SSW events and the ionospheric responses at equatorial, low, and middle latitudes remain poorly understood (Bessarab et al., 2012; Chau et al., 2012; Fang et al., 2014). The SSW events were first observed by Scherhag (1952). They are large meteorological processes in the middle atmosphere polar winter with large and rapid changes in the temperature (Fejer et al., 2011; Fang et al., 2012; Labitzke, 1981). These events are generated by the interaction of planetary waves with zonal mean flow (Matsuno, 1971; 2015; Nath, Sridharan, & Gadhavi, 2015). During an SSW event, the polar vortex of eastward winds in the polar winter could abruptly slow down (minor warming) or reverses their direction (major warming) (Chau, Fejer, & Goncharenko, 2009; Coster, Goncharenko, & Valladares, 2011).

Chau et al. (2012) have published an excellent review of the ionospheric effects at equatorial and low-latitude regions during SSW events. According to Chau et al. (2012), during the SSW events significant changes have been observed in the ionosphere mainly in the zonal electric fields (e.g., Anderson & Araujo-Pradere, 2010; Fejer et al., 2010), total electron content (TEC) (e.g., Chau et al., 2010; Goncharenko et al., 2010; Goncharenko et al., 2010; Liu et al., 2011; Paes et al., 2014), and *F* region critical frequency (f_oF_2) (e.g., Pancheva & Mukhtarov, 2011; Yue et al., 2010). Significant changes in the equatorial ionization anomaly (EIA) during the SSW events have been reported (Fagundes et al., 2015; Goncharenko et al., 2010; Pedatella & Forbes, 2010). Pedatella and Forbes (2010) observed both nonmigrating and migrating perturbations to the semidiurnal tides in the EIA crest region during the SSW events. De Paula et al. (2015) have reported that the SSW events affected the occurrence of the ionospheric irregularities over a low-latitude station in the Brazilian sector.

The equatorial electrojet (EEJ) is a narrow band of intense eastward electrical current system that flows during the daytime above the magnetic dip equator in the ionospheric E layer (Siddiqui et al., 2015; Shume et al., 2010; Sridharan, Sathishkumar, & Gurubaran, 2009; Vineeth, Pant, & Sridharan, 2009). The EEJ current reversal, during the morning and afternoon hours, is named as "counterelectrojet (CEJ)" (Denardini et al., 2009; Fejer et al., 2010; Vineeth et al., 2009). Fejer et al. (2010) have observed that the occurrence of CEJ during SSW events is associated with the enhanced semidiurnal lunar tide. Yamazaki et al. (2012) proposed that the abnormally large lunar tidal winds played a significant role to produce the CEJ during the SSW periods. In a subsequent work, Upadhayaya and Mahajan (2013) have reported significant changes in the EEJ strength during the SSW periods. Although these investigations have provided relevant information about the effects observed in the ionospheric region during the SSW periods, our understanding of the response of equatorial and low-latitude F layer variations during the SSW events remains rather incomplete. Therefore, further studies in this field will greatly help to improve our knowledge about the complex coupling processes between the ionosphere and the lower atmosphere.

In the present work we investigated the ionospheric response in the equatorial and low-latitude regions in the Brazilian sector during to the 2014 SSW events. The basic objectives of this paper are to investigate the variations in the vertical total electron content (VTEC) and EEJ, the generation or suppression of the equatorial ionospheric irregularities and the ionospheric F region electrodynamics in the Brazilian sector during the SSW events that occurred from 02 February 2014 to 20 April 2014 (from day of year (DOY) 33 to 110). Although the 2014 SSW events were characterized by increases in solar flux and geomagnetic disturbance, the forcing due to the SSWs event were quantitatively identified in this study.

2. Data Analysis

In this study, vertical total electron content (VTEC) and phase fluctuations (rate of change of TEC) from several GPS receivers in the Brazilian sector, during the period from 01 January to 30 May 2014 (DOY 01–150), are presented. The wavelet transform was used to construct a time-frequency representation of the hourly average of VTEC and EEJ during DOY 01–150. This wavelet technique provides a good balance between time and frequency localizations (Grinsted, Moore, & Jevrejeva, 2004; Torrence & Compo, 1998).

The VTEC is obtained by applying an obliquity factor $[M(\gamma)]$ to slant total electron content (slant TEC) (Rao et al., 2006):

$$\text{VTEC} = \frac{\text{slant TEC} - (R_{\text{bias}} + S_{\text{bias}})}{M(\gamma)} \qquad (1)$$

where R_{bias} and S_{bias} are the interfrequency differential receiver and satellite biases, respectively. The mapping function $[M(\gamma)]$ is given by (Fedrizzi et al., 2002; Mannucci et al., 1993)

$$M(\gamma) = \frac{1}{\cos(\beta)} = \left\{ 1 - \left(\frac{R_{\text{Earth}} \times \cos(\gamma)}{R_{\text{Earth}} + h} \right)^2 \right\}^{-0.5} \qquad (2)$$

where β is the zenith angle of the GPS satellite at the ionospheric pierce point, R_{Earth} is the radius of the Earth, h is the height of the maximum electron density (here defined as 350 km), and γ is the elevation angle of the line of sight from the receiver to the satellite.

The rate of change of TEC (ROT) has been used to investigate the ionospheric irregularities. As discussed by Aarons, Mendillo, and Yantosca (1996, 1997) and Aarons et al. (2000), the phase fluctuation or ROT is computed at 1 min intervals:

$$\text{ROT} = d\text{TEC}/dt \qquad (3)$$

The ion density measurements on board the Communication/Navigation Outage Forecasting System (C/NOFS) satellite were obtained from the Goddard Space Flight Center NASA online data service (http://cdaweb.gsfc.nasa.gov/istp_public/). This satellite was launched in April 2008 into a low-inclination (13°) orbit with apogee and perigee at ~800 and 400 km, respectively (Bilitza et al., 2012; Burke et al., 2009). As mentioned by De La Beaujardière et al. (2004) and Aveiro et al. (2012), the C/NOFS satellite is dedicated to investigate and forecast the F region irregularities in the equatorial ionosphere.
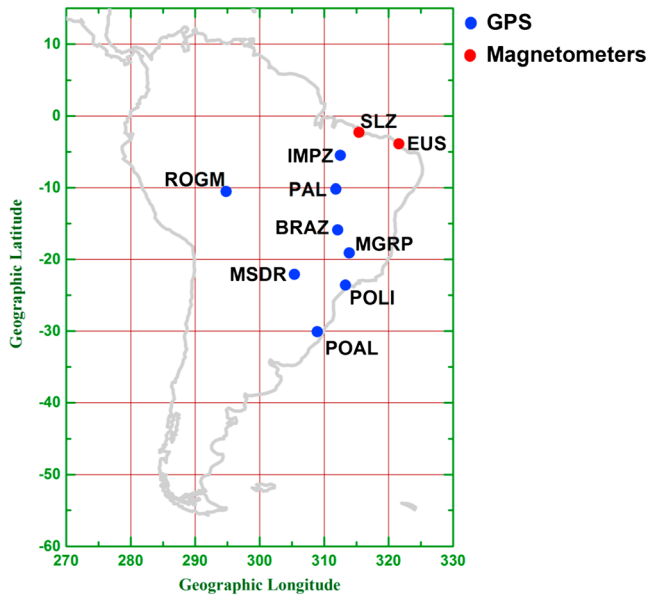
Figure 1. South American map showing the locations of the GPS receivers and magnetometers.

The *Dst* index values are downloaded online from World Data Center, Kyoto (http://wdc.kugi.kyoto-u.ac.jp/dstdir/). The *Kp* index and solar index $F_{10.7}$ were obtained from the websites http://ftp.gwdg.de./pub/geophys/kp-ap/tab/ and http://omniweb.gsfc.nasa.gov/form/dx1.html, respectively. The stratospheric parameters (temperature at 90°N and 10 hPa, and zonal mean wind at 60°N and 10 hPa) were collected from the website http://acdb-ext.gsfc.nasa.gov/Data_services/met/ann_data.html. All data were collected during the 2014 SSW events which occurred from 02 February to 20 April 2014 (from DOY 33 to DOY 110; see Figure 2). In order to generate the historical mean of the stratospheric temperature, usually, all available data by NOAA satellite from 1979 to the year of occurrence of the SSW are considered. Therefore, in the present study, the 36 year median values of the stratospheric temperatures are computed to compare with the stratospheric temperature during the SSW events.

In order to explore the equatorial electrojet (EEJ) variability during the 2014 SSW events we analyzed the horizontal component (*H*) of the Earth's magnetic field observed at São Luis (dip angle of 02.84°S) and Eusébio (dip angle of 07.84°S), Brazil (data provided by the Estudo e Monitoramento Brasileiro do Clima Espacial/Instituto Nacional de Pesquisas Espaciais network). The horizontal component values of the geomagnetic field at the above two locations were normalized according to the equation

$$\Delta H = H - H_{mean} \qquad (4)$$

where *H* is the horizontal component values and H_{mean} is the mean midnight values of the *H* component for the five quietest days in a month (Denardini et al., 2009). In this work we will use the following expression as a proxy to the equatorial electrojet current:

$$EEJ = \Delta H_{SL} - \Delta H_{EUS} \qquad (5)$$

where ΔH_{SL} is the ΔH variations observed at São Luis (station under the EEJ influence) and ΔH_{EUS} is the ΔH variations observed at Eusébio (station outside the EEJ influence). The detailed locations of the GPS and magnetometer stations are shown in Figure 1, and their coordinates are given in Table 1.

Additionally, the data of the VTEC and EEJ during 2015 were used to remove the seasonal effect of the VTEC and EEJ during 2014 (for more details, see equations (6) and (8) of the next section). $F_{10.7}$ mean values between January to April 2014 and January to April 2015 are 153.7 and 129.5, respectively.

Table 1
Details of the Global Positioning System (GPS) and Magnetometer Station Codes, Dip Latitudes, Geographic Latitudes, and Geographic Longitudes Used in the Present Study

Location	Station code (network)[a]	Instrumentation	Geographic latitude	Geographic longitude	Dip latitude
São Luís	SLZ (EMBRACE/INPE)	Magnetometer	02.3°S	315.4°E	02.84°S
Eusébio	EUS (EMBRACE/INPE)	Magnetometer	03.9°S	321.6°E	07.84°S
Imperatriz	IMPZ (RBMC)	GPS	05.5°S	312.5°E	04.10°S
Palmas	PAL (RBMC)	GPS	10.2°S	311.8°E	07.86°S
Guajará-Mirim	ROGM (RBMC)	GPS	10.5°S	294.8°E	0.5°S
Brasília	BRAZ (RBMC)	GPS	15.9°S	312.1°E	12.88°S
Rio Paranaíba	MGRP (RBMC)	GPS	19.2°S	313.9°E	16.58°S
Dourados	MSDR (RBMC)	GPS	22.1°S	305.4°E	14.5°S
São Paulo	POLI (RBMC)	GPS	23.6°S	313.3°E	19.60°S
Porto Alegre	POAL (RBMC)	GPS	30.1°S	308.9°E	21.95°S

[a]EMBRACE/INPE = Estudo e Monitoramento Brasileiro do Clima Espacial/Instituto Nacional de Pesquisas Espaciais, RBMC = Rede Brasileira de Monitoramento Continuo dos sinais GPS.
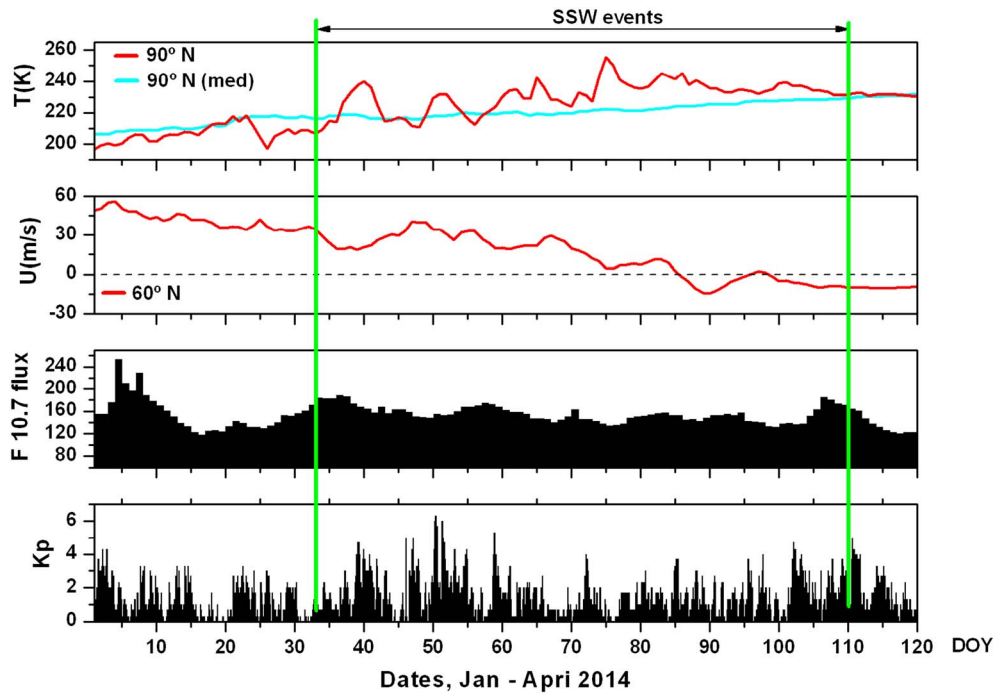
Figure 2. Stratospheric temperature variations at 90°N and 10 hPa, zonal mean wind at 60°N and 10 hPa, $F_{10.7}$ index, and Kp index during DOY 01 to 120. The region included between the green vertical lines indicates the period of the 2014 SSW events. The blue line illustrates the 36 year (1979–2014) mean temperature.

3. Results and Discussion

Figure 2 shows the stratospheric, solar, and geomagnetic conditions during the period from DOY 01 to DOY 120. The region included between the green vertical lines indicates the period of the 2014 SSW events. The first and second panels shown in red lines are the stratospheric temperature (T) at 90° and 10 hPa and zonal mean wind (U) at 60°N and 10 hPa, respectively. Thirty-six-year (1979–2014) median values of the stratospheric temperature are shown as the solid blue line in the first panel. In the second panel the horizontal dashed line corresponds to the zero level (which marks the reversal of the zonal wind). The third and fourth panels present the $F_{10.7}$ index and Kp index variations, respectively.

Figure 2 also indicates that the stratospheric temperature at 90°N increases from DOY 33 (~207 K) to DOY 40 (~240 K), DOY 48 (~210 K) to DOY 51 (~232 K), DOY 56 (~212 K) to DOY 65 (~242 K), DOY 70 (~224 K) to DOY 75 (~256 K), DOY 80 (~235 K) to DOY 83 (~245 K), and from DOY 97 (~232 K) to DOY 101 (~240 K). This indicates that five SSW events occurred during the period from DOY 33 to DOY 110 of the year 2014, among which, four events are minor SSWs (DOY 40, DOY 50–52, DOY60–65, and DOY 75) and one major SSW event (DOY 86). The fifth SSW event is classified as major warming since the zonal stratospheric wind reverses from eastward to westward on DOY 86. During DOY 04 to DOY 85, the zonal stratospheric wind is gradually slowing down. It is seen from the fourth panel in Figure 2 that the Kp index reached ~6 on DOY 50 and 51. However, in general, the Kp index was below 5 during the 2014 SSW events. It can also be observed that the $F_{10.7}$ index was below 190 units during these SSW events.

The VTEC variations at IMPZ, PAL, ROGM, BRAZ, MGRP, MSDR, POLI, and POAL during DOY 01 to DOY 120 are presented in Figure 3. The gray colored solid vertical lines on DOY 33 and 110 indicate the beginning of the first 2014 SSW event and the end of the fifth 2014 SSW event, respectively. The white colors indicate no data. The gray vertical dashed lines indicate the stratospheric temperature peaks on DOY 40, 51, 62, 65, 75, 83, and 101 during the SSW events. The top plot of Figure 3 shows the Dst index variations during DOY 01 to 120.

Two geomagnetic storms occurred during the period from DOY 49 to DOY 62. The first and second geomagnetic storms are classified as intense and moderate geomagnetic storms, respectively. The intense geomagnetic storm occurred with a minimum Dst value of −116 nT at 9 UT on DOY 50, and the moderate geomagnetic storm is seen with a minimum Dst value of −94 nT at 0 UT on DOY 59. Figure 3 also shows
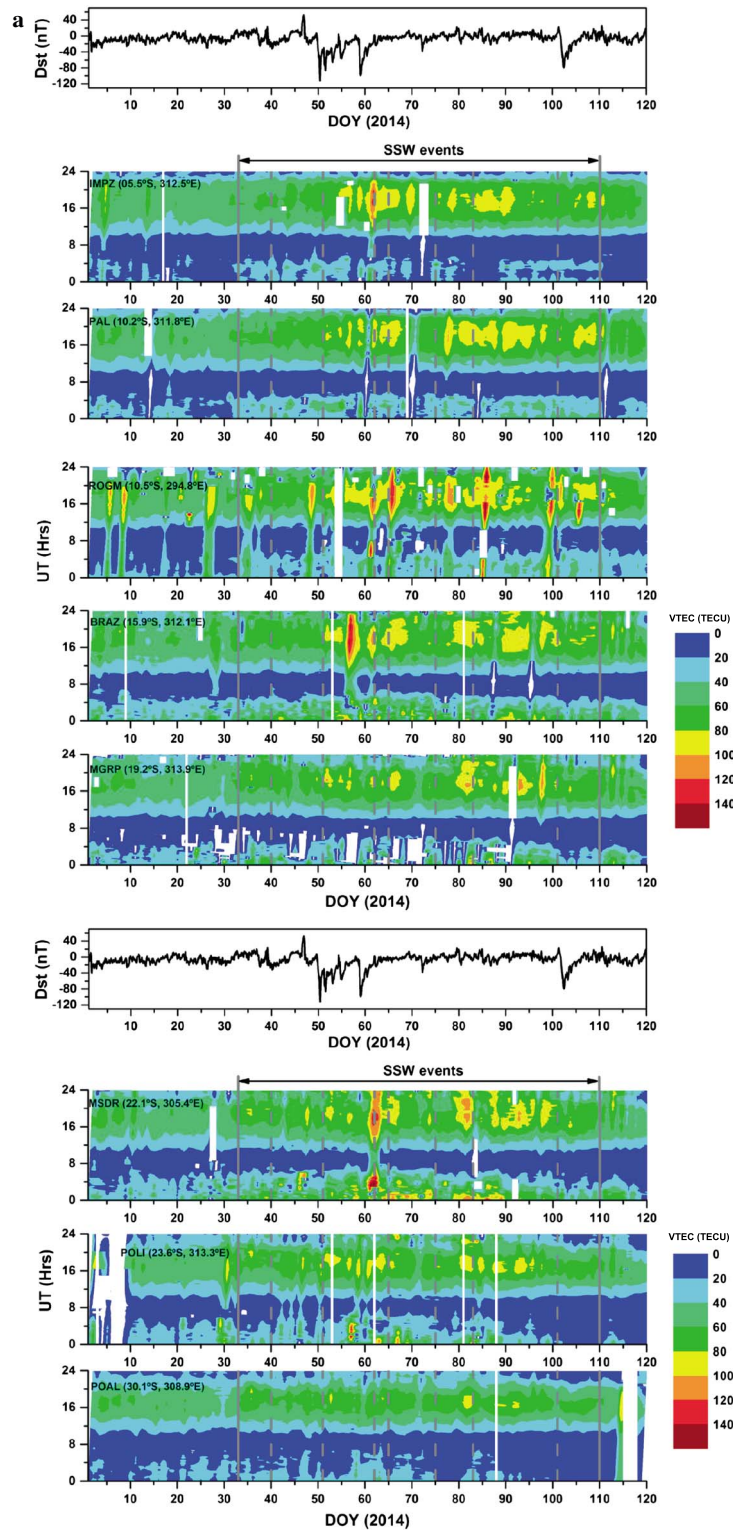
Figure 3. (a) VTEC variations at IMPZ, PAL, ROGM, BRAZ, MGRP, MSDR, POLI, and POAL during DOY 01–120. The white colors indicate no data. The gray vertical lines indicate the onset (on DOY 33) and end (on DOY 110) of the first and fifth 2014 SSW events, respectively. The gray vertical dashed lines on DOY 40, 51, 62, 65, 75, 83, and 101 indicate the SSW temperature peaks. Also, the diurnal (UT) variations of the *Dst* index for the period DOY 01–120 are presented. (b) UT variations of the VTEC at IMPZ, PAL, BRAZ, MGRP, and MSDR during DOY 73, 74, 76, 79, 80, 84, 86, and 90. The average of the observations during DOY 01–32 is shown as gray bands with ±1 standard deviation.
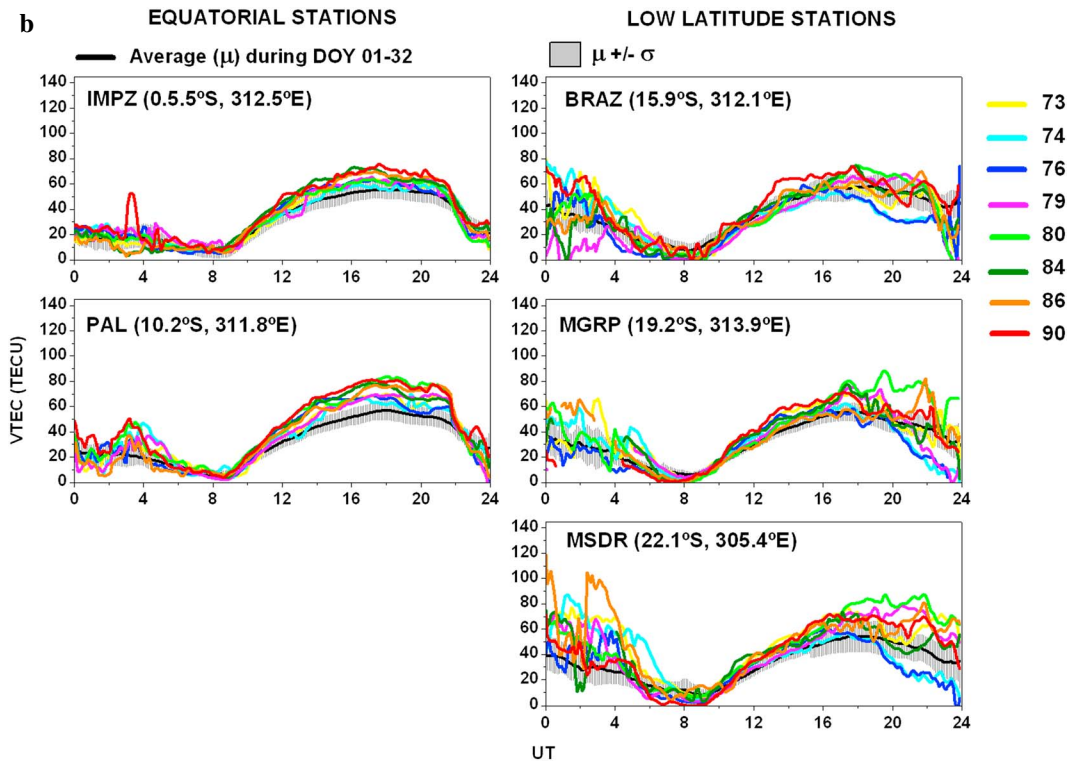
Figure 3. (continued)

that a moderate geomagnetic storm occurred during DOY 100 to 106. During this moderate geomagnetic storm Dst reached a minimum value of −81 nT at 10 UT on DOY 102.

In general, during DOY 51 to DOY 110 (after the second SSW temperature peak), Figure 3 shows a significant increase in VTEC at IMPZ, PAL, ROGM (equatorial stations), BRAZ, MGRP, MSDR, and POLI (low-latitude stations) around 15–22 UT, compared with undisturbed days (taken before the SSW events). The maximum TEC observed during the geomagnetic storms (DOY 49–62 and DOY 100–106) is broad, in general, varying between 80 and 140 total electron content unit, 1 TECU = 10^{16} el m^{-2} (see Figure 3). In order to highlight the VTEC diurnal characteristics during the 2014 SSW events and outside the magnetic storm period, a comparison between the VTEC$_{new}$ (see equation (6)) during DOY 73, 74, 76, 79, 80, 84, 86, and 90 (SSW days) with the VTEC variations before the SSW events is shown in Figure 3b for equatorial and low-latitude stations. The effects of seasonal variations of VTEC (2014) were removed using the following equation:

$$VTEC_{new} = VTEC_{2014} - \left(VTEC_{March\ 2015} - VTEC_{January\ 2015}\right) \tag{6}$$

where VTEC$_{2014}$ is the VTEC value during DOY 73, 74, 76, 79, 80, 84, 86, and 90 (2014) at each location and VTEC$_{March\ 2015}$ and VTEC$_{January\ 2015}$ are the mean values of VTEC of the corresponding stations for 10 quietest days in March and January (2015), respectively. The average daily variations (obtained during DOY 01 to 32; before the SSWs) of VTEC are shown in Figure 3b as gray bands, and its width corresponds to ±1 standard deviation.

The diurnal variations presented in Figure 3b indicate increases in VTEC at equatorial and low-latitude regions between 15 and 22 UT during DOY 73–90. We computed the VTEC mean value between 15 and 22 UT (see Table 2) during DOY 01–32 (VTEC$_{average}$; before the SSWs) and VTEC$_{new}$ mean value between 15 and 22 UT on DOY 73–90 (during the SSWs). The percentage of deviations in VTEC (%) for DOY 73, 74, 76, 79, 80, 84, 86, and 90 (Table 2) is computed using the following expression:

$$VTEC\ (\%) = 100 \times \left(VTEC_{DOY} - VTEC_{average}\right)/VTEC_{average} \tag{7}$$

where VTEC$_{DOY}$ is the VTEC$_{new}$ mean value (15–22 UT) for each DOY. Table 2 shows a mean VTEC increase for the equatorial region of about 17%, 12%, 14%, 19%, 27%, 28%, 30%, and 36% during DOY 73, 74, 76, 79, 80,

Table 2
Details of the VTEC (15–22 UT) Used in Figure 3b

Station code	Average DOY 01–32	DOY 73	DOY 73 (%)	DOY 74	DOY 74 (%)	DOY 76	DOY 76 (%)	DOY 79	DOY 79 (%)
Equatorial region									
IMPZ	52.6	58.8	11.8	56.6	7.6	57.8	9.8	59.6	13.4
PAL	52.5	64.5	22.8	61.2	16.5	61.9	17.8	65.6	24.9
Mean (equatorial)	52.6	61.6	17.3	58.9	12.1	59.8	13.8	62.6	19.1
Low-latitude region									
BRAZ	54.8	53.9	−1.7	42.1	−23.2	43.1	−21.3	61.0	11.4
MGRP	50.6	56.9	12.3	47.4	−6.5	46.2	−8.8	57.9	14.3
MSDR	49.9	64.0	28.1	42.9	−14.0	44.9	−10.0	67.7	35.7
Mean (low latitude)	51.8	58.2	12.9	44.1	−14.6	44.7	−13.4	62.2	20.5

Station code	Average DOY 01–32	DOY 80	DOY 80 (%)	DOY 84	DOY 84 (%)	DOY 86	DOY 86 (%)	DOY 90	DOY 90 (%)	Average DOY 73–90	Average DOY 73–90 (%)
Equatorial region											
IMPZ	52.6	59.4	13.0	64.8	23.1	64.8	23.2	67.4	28.2	61.2	16.3
PAL	52.5	74.3	41.4	69.8	32.8	71.6	36.3	75.4	43.5	68.0	29.5
Mean (equatorial)	52.6	66.9	27.2	67.3	28.0	68.2	29.8	71.4	35.8	64.6	22.9
Low-latitude region											
BRAZ	54.8	64.1	16.9	59.1	7.9	57.6	5.1	62.0	13.2	55.4	1.0
MGRP	50.6	72.3	42.8	56.8	12.2	55.0	8.6	60.3	19.0	56.6	11.8
MSDR	49.9	75.9	52.1	56.1	12.3	63.0	26.2	66.3	32.7	60.1	20.4
Mean (low latitude)	51.8	70.8	37.3	57.3	10.8	58.5	13.3	62.9	21.6	57.3	11.1

Note. The increase in VTEC in the afternoon (15–22 UT). The averaged VTEC between DOY 01 and DOY 32 ($VTEC_{average}$) and averaged VTEC during DOY 73, 74, 76, 79, 80, 84, 86, and 90 ($VTEC_{DOY}$) are calculated between 15 and 22 UT. The percentage of deviations in VTEC (%) are computed according to equation (7).

84, 86, and 90, respectively. Table 2 also shows that the percentage of deviations in VTEC (%) at low-latitude region is about 13%, −15%, −13%, 21%, 37%, 11%, 13%, and 22% during DOY 73, 74, 76, 79, 80, 84, 86, and 90, respectively. The mean increase in VTEC over equatorial and low latitudes during DOY 73–90 (between 15 and 22 UT) is about 23% and 11%, respectively (for more details, see the last column in Table 2). Apart from the increase in VTEC between 15 and 22 UT (mentioned earlier), Figure 3b shows an increase in VTEC over equatorial and low latitudes around 0–5 UT, and this increase is found to be more pronounced over low-latitude regions. The VTEC mean values during the nighttime period of 0–5 UT are presented in Table 3 in the similar to those presented in Table 2. It is noticed from Table 3 that the percentage of deviations in VTEC (%) at equatorial region (between 0 and 5 UT) are about −6%, 29%, 13%, 16%, 19%, −29, −25%, and 50% during DOY 73, 74, 76, 79, 80, 84, 86, and 90, respectively. Table 3 also demonstrates that the percentage of deviations in VTEC (%) at low-latitude region (0–5 UT) is about 65%, 73%, 3%, −18%, 35%, 27%, 68%, and 12% on DOY 73, 74, 76, 79, 80, 84, 86, and 90, respectively. The last column in Table 3 shows a mean VTEC increase for the equatorial and low-latitude regions of about 8% and 33%, respectively, between 0 and 5 UT. de Jesus et al. (2017), Goncharenko et al. (2010), Fagundes et al. (2015), and Vieira et al. (2017) have investigated the ionospheric response to the 2006, 2008, 2009, and 2012 SSW events, respectively, using GPS-TEC measurements in the South American sector (equatorial and low-latitude regions). Liu et al. (2011) have studied the equatorial electrodynamics and neutral background in the Asian sector (equatorial and low-latitude regions) during the 2009 major SSW event, using GPS-TEC observations. de Jesus et al. (2017) have studied the response of the ionospheric F region in the equatorial and low-latitude regions over South American and African sectors during the 2012 minor SSW event. Goncharenko et al. (2010), Liu et al. (2011), Fagundes et al. (2015), de Jesus et al. (2017), de Jesus et al. (2017), and Vieira et al. (2017) have reported that the TEC was decreased in the afternoon during the SSW event. However, our results showed (for the first time) that the electron density was intensified in the afternoon during the 2014 SSW events. The intensification of the electron density is associated with the occurrence of the 2014 SSW events, but it could also be linked to solar flux and seasonal change during this period. In addition, the perturbations (intensifications) in VTEC can be due the changes in the E layer electric fields during the 2014 SSW events. According to Goncharenko et al. (2010), the interaction of planetary waves with the tidal fields creates an enhancement in the semidiurnal tide in the lower

Table 3
Details of the VTEC (0–5 UT) Used in Figure 3b

Station code	Average DOY 01–32	DOY 73	DOY 73 (%)	DOY 74	DOY 74 (%)	DOY 76	DOY 76 (%)	DOY 79	DOY 79 (%)
				Equatorial region					
IMPZ	17.2	14.8	−14.0	21.9	27.2	20.1	16.7	21.4	24.1
PAL	21.2	21.8	2.6	27.6	29.8	23.3	9.4	22.8	7.4
Mean (equatorial)	19.2	18.3	−5.7	24.8	28.5	21.7	13.1	22.1	15.7
				Low-latitude region					
BRAZ	31.4	46.7	48.8	51.3	63.3	31.2	−0.7	11.4	−63.5
MGRP	27.3	35.3	29.3	39.2	43.6	20.5	−24.8	10.5	−61.4
MSDR	30.5	66.1	117.0	64.4	111.4	41.2	35.4	51.7	69.8
Mean (low latitude)	29.7	49.4	65.0	51.6	72.8	31.0	3.3	24.6	−18.4

| Station code	Average DOY 01–32	DOY 80	DOY 80 (%)	DOY 84	DOY 84 (%)	DOY 86	DOY 86 (%)	DOY 90	DOY 90 (%)	Average DOY 73–90	Average DOY 73–90 (%)
				Equatorial region							
IMPZ	17.2	17.8	3.3	12.2	−29.4	11.6	−32.7	24.2	40.4	18.0	4.4
PAL	21.2	28.5	34.3	No data	No data	17.8	−16.4	33.8	59.1	25.1	18.0
Mean (equatorial)	19.2	23.2	18.8	12.2	−29.4	14.7	−24.6	29.0	49.7	20.7	8.3
				Low-latitude region							
BRAZ	31.4	38.8	23.6	27.4	−12.7	31.8	1.2	47.2	50.3	35.7	13.8
MGRP	27.3	35.1	28.6	37.5	37.5	47.3	73.3	15.6	−42.7	30.1	10.4
MSDR	30.5	46.5	52.5	47.9	57.3	70.2	130.4	38.8	27.3	53.4	75.1
Mean (low latitude)	29.7	40.1	34.9	37.6	27.4	49.8	68.3	33.9	11.6	39.7	33.1

Note. VTEC variations during 0–5 UT. The averaged VTEC between DOY 01 and DOY 32 (VTEC$_{average}$) and averaged VTEC during DOY 73, 74, 76, 79, 80, 84, 86, and 90 (VTEC$_{DOY}$) are calculated between 0 and 5 UT. The percentage of deviations in VTEC (%) are computed using the following equation: VTEC (%) = $100 \times$ (VTEC$_{DOY}$ − VTEC$_{average}$)/VTEC$_{average}$.

thermosphere. Enhanced tidal winds in the *E* region modulate the *E* layer electric fields via *E* layer dynamo field, which is mapped from the *E* region to the *F* layer along the magnetic field lines (Goncharenko et al., 2010). This complicated interaction between the *E* and *F* layers generates the equatorial electric fields, which control the vertical plasma drift in the *F* region (Fagundes et al., 2015; Fejer et al., 1979). This discrepancy between our results and the observations of Goncharenko et al. (2010), Liu et al. (2011), Fagundes et al. (2015), de Jesus et al. (2017), de Jesus et al. (2017), and Vieira et al. (2017) is possibly associated to the difference in the intensity of solar activity during each SSW event. The solar activity was very low during the 2006, 2008, and 2009 SSW events ($F_{10.7}$~70–80 W m^{-2} Hz). In the case of the 2012 SSW event, solar flux was moderate ($F_{10.7}$~130 W m^{-2} Hz). In the present study, the solar activity was high ($F_{10.7}$~175 W m^{-2} Hz; see Figure 2). According to Vieira et al. (2017), during the 2012 SSW event, combination of lower solar flux and seasonal change can be responsible for ~15% perturbation in VTEC, and the SSW event is responsible for the rest of the perturbation in TEC. However, more investigations (during high solar activity) are needed to improve our knowledge of the VTEC increase at equatorial and low-latitude regions during the SSW events.

The second and fourth panels in the Figure 4a show the UT variations of the EEJ ground strength (from DOY 01 to 120) during 2014 and 2015, respectively. The white colors indicate no data. In the second panel the onset time of the first SSW event and the end time of the fifth SSW event are indicated by the gray vertical lines on DOY 33 and DOY 110, respectively. The vertical dashed lines (second panel) on DOY 40, 51, 62, 65, 75, 83, and 101 indicates the SSW temperature peaks. The first and third panels in Figure 4a show the time variations of the *Dst* index (DOY 01–120) during 2014 and 2015, respectively.

The proxy values used for EEJ vary between −20 and 10 nT (green, yellow, and orange patterns seen in the second panel in Figure 4a) during the first and second geomagnetic storms (DOY 49–62; 2014). The EEJ proxy observed from DOY 100 to 106 (2014), during the third geomagnetic storm, is varying between −20 and −5 nT (see the second panel in Figure 4a). The third panel in Figure 4a shows that an intense geomagnetic storm occurred during the period from DOY 76 to 83 (2015). This geomagnetic storm reached a minimum *Dst* value of −222 nT at 23 UT on DOY 76 (2015). The proxy values used for EEJ observed during this intense geomagnetic storm (2015) are varying between −5 and 25 nT (fourth panel in Figure 4a). In general, the
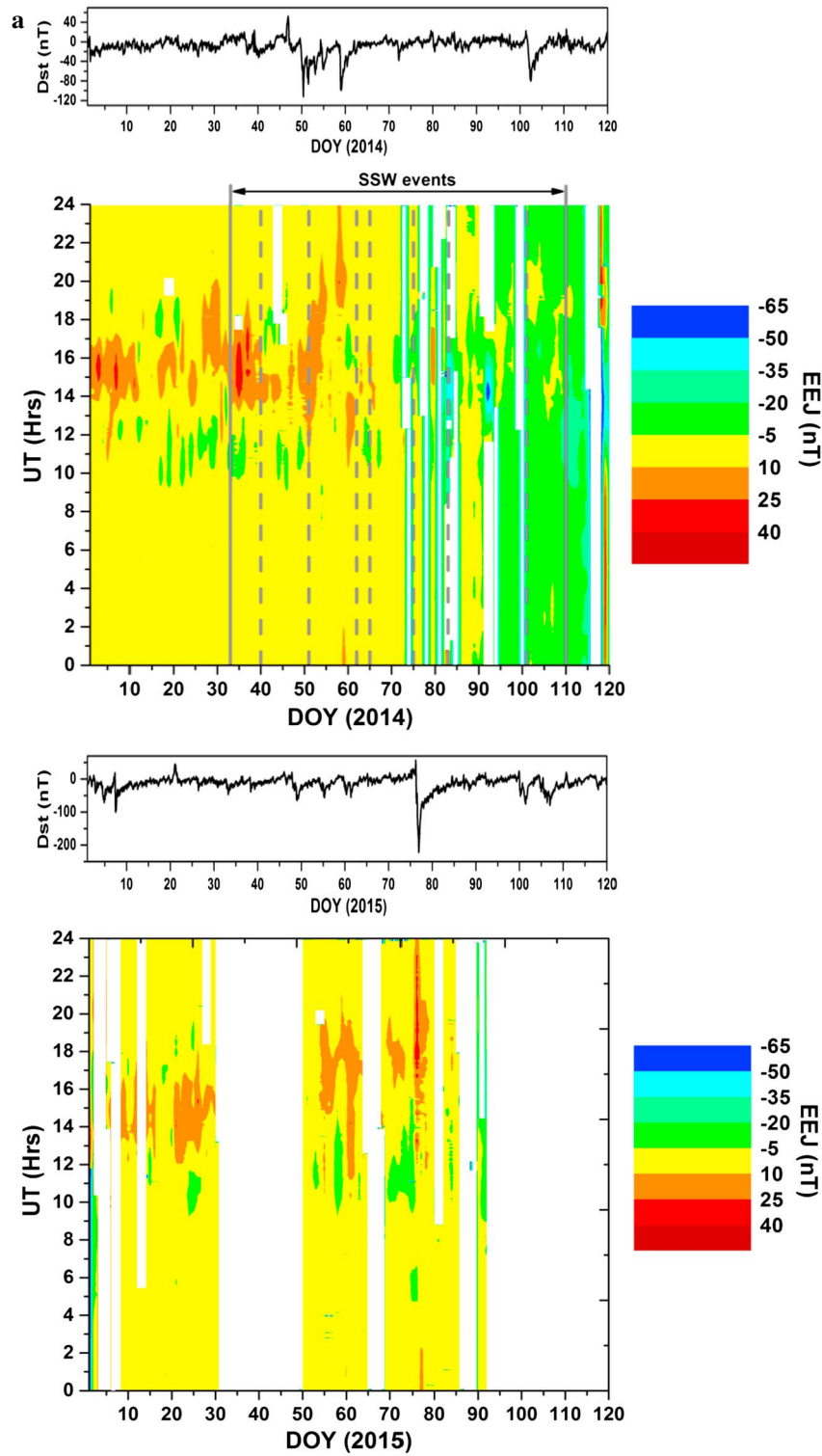
Figure 4. (a) EEJ variations during DOY 01 to 120 (2014 and 2015). The gray vertical lines on DOY 33 and 110 (second panel) indicate the onset of the first SSW and the end of the fifth SSW, respectively. The gray vertical dashed lines on DOY 40, 51, 62, 65, 75, 83, and 101 (second panel) indicate the SSW temperature peaks. The white colors (second and fourth panels) indicate no data. Also, the *Dst* index for the period DOY 01–120 (2014 and 2015) is presented. (b) UT variations of the EEJ during DOY 74, 76, 79, 80, 86, and 90. The average of the observations during DOY 01–32 is shown as gray bands with ±1 standard deviation.
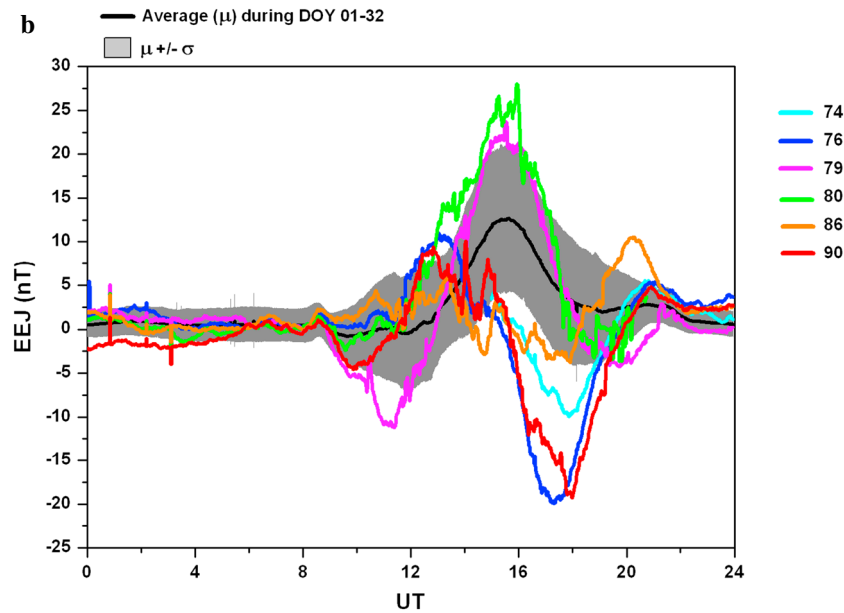
Figure 4. (continued)

second and fourth panels in Figure 4a show an intensification of EEJ (from DOY 01 to 55 around 14–18 UT) during 2014 and 2015, respectively. Day-to-day variations in EEJ are strongly affected by variations in solar and geomagnetic activities. The intensifications of EEJ during DOY 05 and DOY 35 (2014) are probably due to high solar activity, while intensification of EEJ during DOY 50 (2014) is due to storm time effect. Also, the intensification of EEJ around DOY 76–77 (2015) is due to geomagnetic storm.

After the second SSW temperature peak, the second panel in Figure 4a shows a substantial decrease in EEJ in the afternoon (around 14–20 UT) on DOY 55–110 (2014), compared with the previous days. Also, the fourth panel in Figure 4a shows a decrease in EEJ around 14–18 UT on DOY 60–90 (2015), compared with the previous days. However, in general, the decrease in EEJ on DOY 55–85 (around 16 UT) is apparently more significant in 2014 than in 2015. The EEJ after DOY 90 (2014; second panel in Figure 4a) decreased with time possibly due to seasonal change.

In general, the second panel in Figure 4a shows a strong CEJ during DOY 55–110 (2014) around 14–20 UT. The results presented here support our earlier results that there is (in general) significant increase in VTEC (equatorial region; see Figure 3) during DOY 55–110 (around 14–20 UT). According to Chakraborty and Hajra (2008), the EEJ strength provides an estimate of the equatorial electric field responsible for the fountain effect. Much larger values of TEC at equatorial stations, contrary to the normal feature, indicate increased electron density at the magnetic equator during the strong westward electric fields (CEJ)—which may be attributed to a poorly formed fountain effect (Hajra, Chakraborty, & Paul, 2009; Joseph et al., 2015). In the present investigations, the effects of seasonal variations of EEJ during 2014 were removed using the following relation:

$$EEJ_{new} = EEJ_{2014} - \left(EEJ_{March\ 2015} - EEJ_{January\ 2015}\right) \tag{8}$$

where EEJ_{2014} is the EEJ value on DOY 74, 76, 79, 80, 86, and 90 (2014) and $EEJ_{March\ 2015}$ and $EEJ_{January\ 2015}$ are the mean values of EEJ for 10 quietest days in March and January 2015, respectively. In order to highlight the EEJ changes during the SSW events and outside the storm period, the EEJ_{new} variations on DOY 74, 76, 79, 80, 86, and 90 are presented in Figure 4b. The average EEJ variations for undisturbed period (DOY 01–32; taken before the SSWs) are shown with gray band, and its width corresponds to ±1 standard deviation.

Figure 4b shows a very strong CEJ on DOY 74, 76, 79, 86, and 90 during the daytime period. Figure 4b also shows the enhanced EEJ on DOY 79, 80 (around 14–16 UT), and 86 (around 19 UT). The EEJ mean values from 14 to 20 UT during DOY 01–32 ($EEJ_{average}$; before the SSWs) and EEJ_{new} mean values (14–20 UT) on DOY 74, 76, 79, 80, 86, and 90 (SSW days) are shown in Table 4. The percentage of deviations in EEJ (%) for DOY 74, 76, 79, 80, 86, and 90 are calculated using the following equation:

Table 4
Details of the EEJ (14–20 UT) Used in Figure 4b

Parameter	Average DOY 01–32	DOY 74	DOY 74 (%)	DOY 76	DOY 76 (%)	DOY 79	DOY 79 (%)		
EEJ	6.7	−3.2	−147.6	−7.0	−203.8	9.3	39.5		
Parameter	Average DOY 01–32	DOY 80	DOY 80 (%)	DOY 86	DOY 86 (%)	DOY 90	DOY 90 (%)	Average DOY 74–90	Average DOY 74–90 (%)
EEJ	6.7	11.3	69.0	0.7	−89.6	−6.0	−190.1	0.9	−87.1

Note. The EEJ variations in the afternoon (14–20 UT). The averaged EEJ between DOY 01 and DOY 32 (EEJ$_{average}$) and averaged EEJ during DOY 74, 76, 79, 80, 86, and 90 (EEJ$_{DOY}$) are calculated between 14 and 20 UT. The percentage of deviations in EEJ (%) are computed according to equation (9).

$$EEJ \quad (\%) = 100 \times \left(EEJ_{DOY} - \ EEJ_{average}\right)/EEJ_{average} \qquad (9)$$

where EEJ$_{DOY}$ is the EEJ$_{new}$ mean value (14–20 UT) for every DOY. Table 4 shows that the percentage of deviations in EEJ (%), between 14 and 20 UT, is about −148%, −204%, 40%, 69%, −90%, and −190% on DOY 74, 76, 79, 80, 86, and 90, respectively. It can be noticed from the last column in Table 4 that the average percentage of deviation in EEJ during DOY 74–90 gives negative values (−87%) since the mean EEJ before the SSWs is larger than that during the SSWs, which reinforces the EEJ reduction during the SSW days. Earlier studies (de Jesus et al., 2017; Sridharan et al., 2009; Upadhayaya & Mahajan, 2013) have reported significant perturbations in the EEJ associated with the occurrence of SSW events. Sridharan et al. (2009) have reported a CEJ in the Indian sector during the SSW events that occurred in the winter months of 1998–1999, 2001–2002, 2003–2004, and 2005–2006. Upadhayaya and Mahajan (2013) observed a CEJ in the Asian sector during the 2008 SSW event. Our present investigations during the 2014 SSW events are in agreement with the recent studies. According to Rastogi (1999), the CEJ events during the northern winter months result from changes in the wind system (in the ionosphere) related with the SSW events. Yamazaki et al. (2012) suggested that abnormally large lunar tidal winds may play an important role in the day-to-day variability of the EEJ during the SSW events.

Figures 5 and 6 show the wavelet plots of hourly average of VTEC (from several stations) and EEJ, respectively, during DOY 01 to 150. The thick black contours indicate the significant regions (at the 5% level) against random noise. The green vertical lines on DOY 33 and 110 indicate the beginning of the first SSW event and the end of the fifth SSW event, respectively. The white colors indicate no data.

Figure 5 shows that the wavelet power spectrum of VTEC is broadly distributed at equatorial and low-latitude stations during the SSW events, mainly in the 0.25 to 16 day band. The continuous wavelet transform (CWT) of VTEC (Figure 5) in general revealed strong 12 h and 24 h periodicities at the equatorial and low-latitude regions during the 2014 SSW events. However, the diurnal (24 h) periodicity is usually noticed in other periods also (see Figure 5) and might not be related with the occurrence of the SSW events. During the SSW events, the CWT of EEJ strength (see the thick black contours in Figure 6) clearly shows the presence of oscillations with periods of about 0.25–1 day and 0.25–2 days on DOY 33–38 and DOY 82–94, respectively. Apart from the periodicities highlighted by the thick black contours (mentioned earlier), Morlet wavelet analysis of VTEC (Figure 5) and EEJ strength (Figure 6) shows the presence of stronger periods of ~2–16 days during the 2014 SSW events. The 2–16 day components of EEJ are also enhanced during DOY 120 to DOY 130 (after the SSWs; see Figure 6), possibly due to the occurrence of three geomagnetic storms (not shown here) during this period. Semidiurnal perturbation in TEC at low latitudes during the 2009 major SSW event over the American and Asian sectors are reported by Goncharenko et al. (2010) and Liu et al. (2011), respectively. Goncharenko et al. (2010) have also reported a semidiurnal variation in TEC in the American sector during the 2008 SSW events. McDonald, Sassi, and Mannucci (2015) have investigated the SAMI3/SD-WACCM-X simulations of ionospheric variability during the 2009 major SSW event. They reported that nonmigrating tides contributed to a semidiurnal perturbation at the Jicamarca longitudes (285°E) during 2009 major SSW event. Our results show a semidiurnal perturbation in VTEC and EEJ during the SSW events of 2014, which confirmed the results of the previous investigations (Goncharenko et al., 2010; Liu et al., 2011; McDonald et al., 2015) during other SSW events. In the present investigation, the semidiurnal perturbation in VTEC and EEJ was caused by an enhanced semidiurnal variation in the $E \times B$ vertical plasma motion, which could be associated to an amplified semidiurnal nonmigrating tide in the lower thermosphere (Goncharenko et al., 2010;
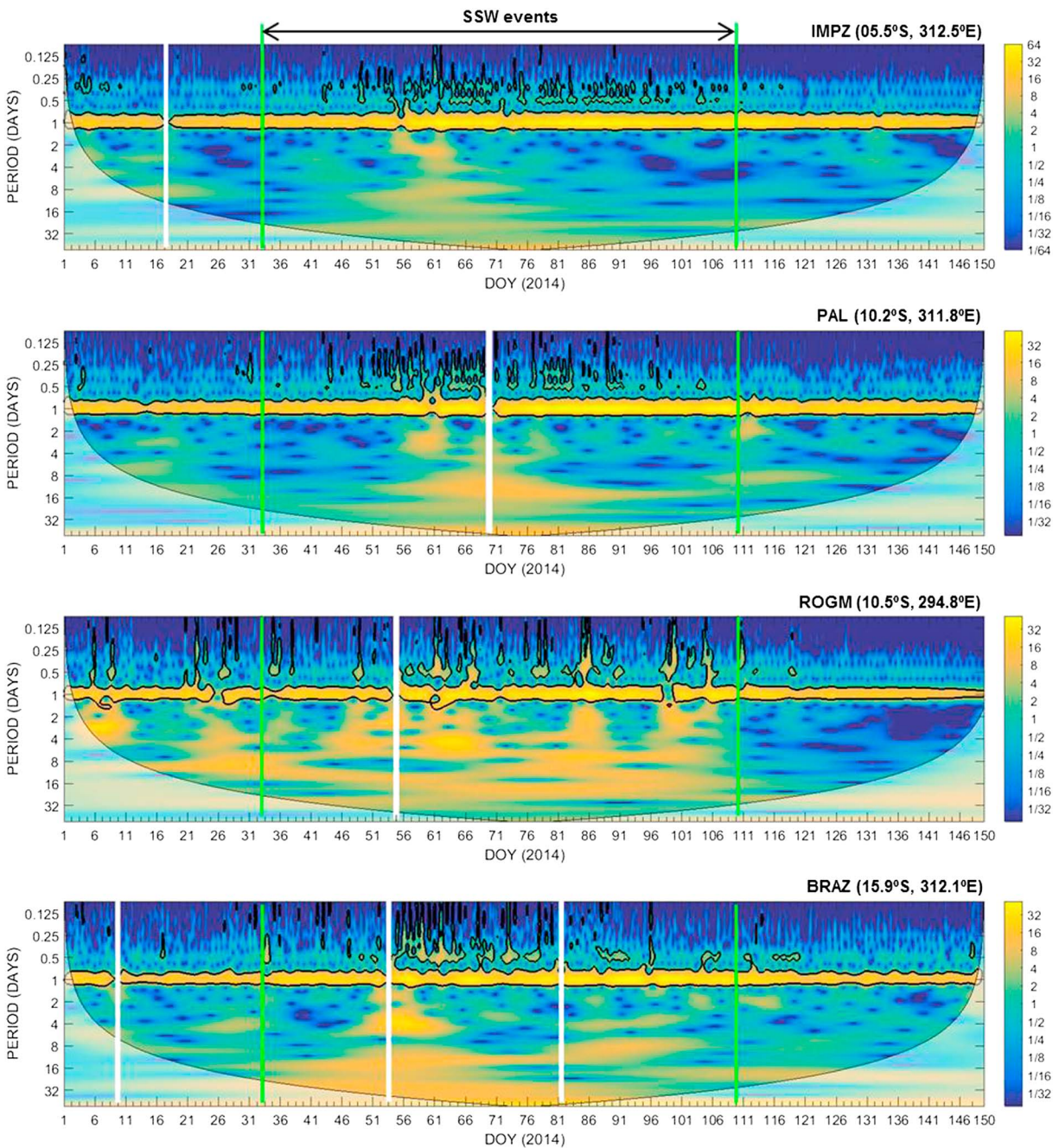
Figure 5. Wavelet transform applied in the hourly average of VTEC during DOY 01 to DOY 150. The white colors indicate no data. The green vertical lines indicate onset (DOY 33) of the first SSW and the end (DOY 110) of the fifth SSW events.

McDonald et al., 2015; Pedatella et al., 2012). Pedatella et al. (2012) carried out an investigation of the tide response to 23 SSW events using model simulations (Whole Atmosphere Community Climate Model) and reported amplification in the migrating and nonmigrating semidiurnal tide during SSW events. According to Goncharenko et al. (2010), an enhancement in the semidiurnal tide in the lower thermosphere during the SSW event is caused due to the interaction between planetary waves, tides, and gravity waves.

Laskar et al. (2013) have investigated the vertical coupling of atmospheric regions during different levels of solar activity, using combined multiwavelength optical dayglow, magnetic, and radio measurements in the Indian sector. They have reported that the coupling of lower and upper atmosphere is weaker during high
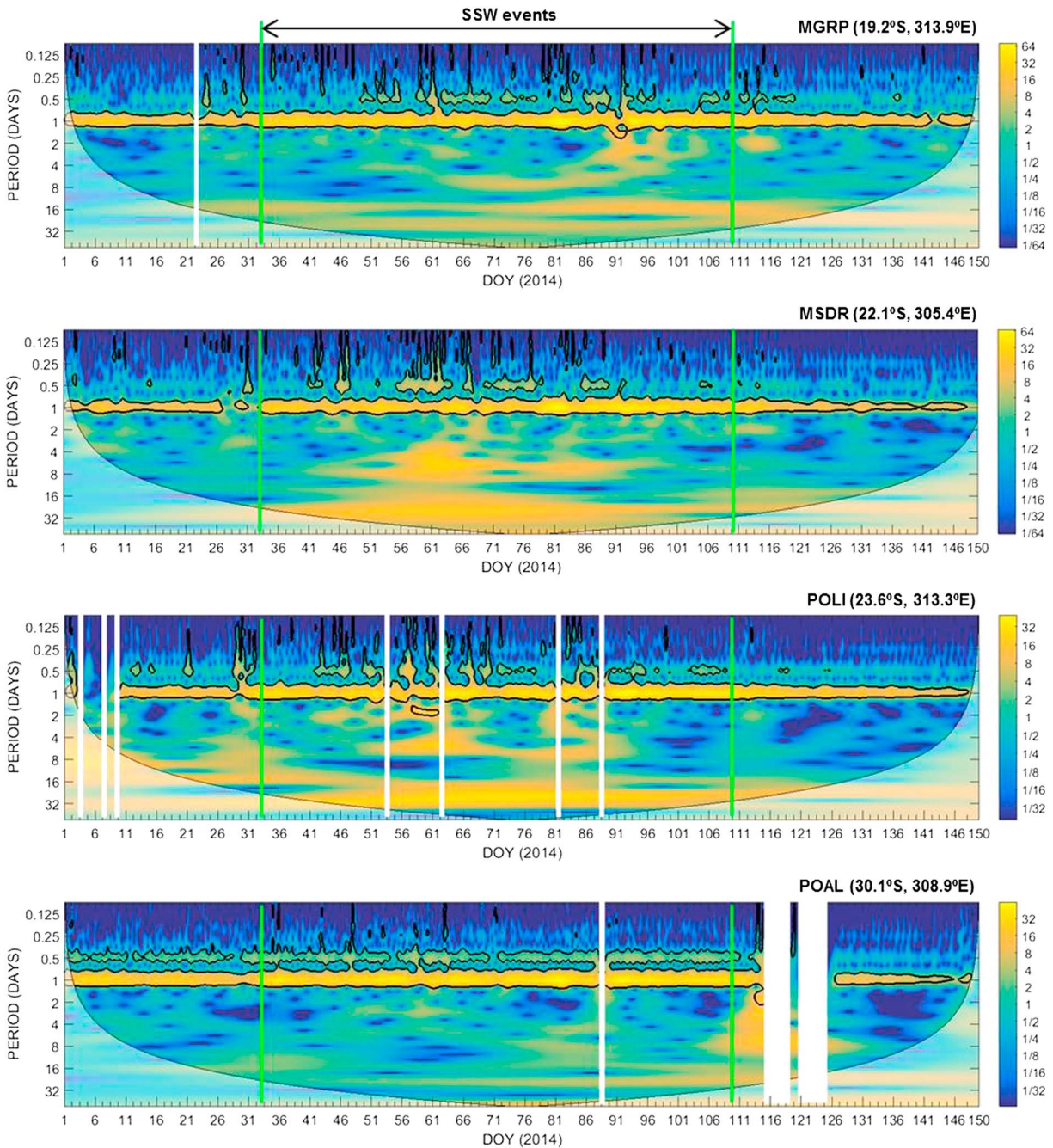
Figure 5. (continued)

solar activity. However, they proposed that the occurrence of SSW events may enhance the coupling from below even during high solar activity. Laskar, Pallamraju, and Veenadhari (2014) have studied the EEJ strength and the TEC data over the Indian sector during the SSW events that occurred between 2005 and 2013. During the 2013 SSW event (a period of high solar activity), Laskar et al. (2014) reported experimental evidence to that hypothesis developed by Laskar et al. (2013). According to Laskar et al. (2013, 2014), the SSW events provide additional energy which will considerably affect the upper atmosphere (coupled to the ionosphere), irrespective of the levels of solar activity. Laskar et al. (2014) have reported the presence of 2 to 25 day periods in the EEJ and TEC (Indian sector) during the SSW events. However, the most dominant periodicities that have been observed by Laskar et al. (2014) are the periods of 11 to 20 days (quasi 16 day oscillation). Jonah et al. (2014) also observed the amplification of quasi
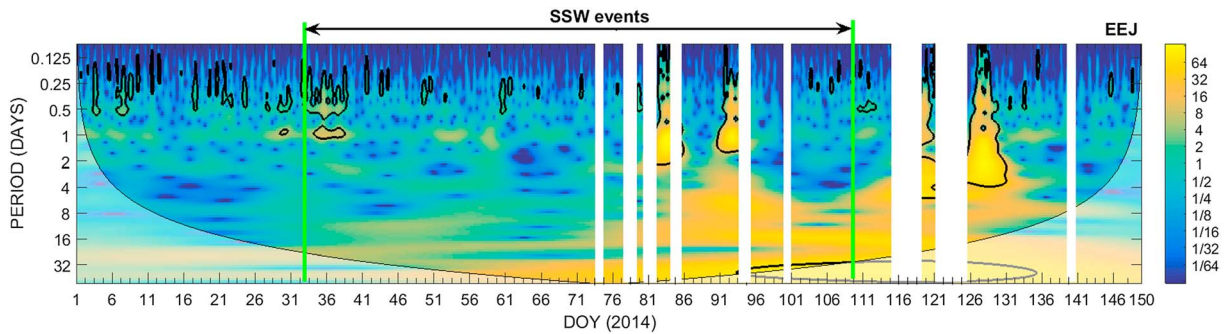
Figure 6. Wavelet transform applied in the hourly average of EEJ from DOY 01 to DOY 150. The white colors indicate no data. The green vertical lines indicate the onset (DOY 33) of the first SSW and the end (DOY 110) of the fifth SSW events.

16 day oscillations in the TEC (Brazilian sector) during the 2013 major SSW event. In the present work, Figures 5 and 6 show an amplification of the quasi 16 day oscillation in the VTEC and EEJ, respectively, during the 2014 SSW events. These results support the observations made by Laskar et al. (2014) and Jonah et al. (2014). Other than the quasi 16 day periods, Figures 5 and 6 show an amplification of the ~2–10 day periods in the EEJ and VTEC (Brazilian sector) during the SSW days. de Jesus et al. (2017) also observed an amplification of the ~2–6 day periods in the VTEC (Brazilian sector) during the 2012 minor SSW event. To the best of our knowledge, our present results show for the first time that SSW events can amplify the ~2–10 day periodicities in EEJ, during a solar activity year as high as this one of 2014. According to Laskar et al. (2014), the periodicities of ~2–20 days observed in TEC and EEJ, during the SSW event, are possibly related with both variabilities of tides and planetary waves from the lower atmosphere. During the SSW events the semidiurnal solar and lunar tides and planetary wave amplitudes are amplified and their combined action significantly affects the ionosphere (Pedatella & Liu, 2013; Laskar et al., 2014).

Figure 7 shows the percentage of nights in which phase fluctuations were observed before (DOY 01–32) and during (DOY 33–110) the SSW events. The phase fluctuations (rate of change of TEC-ROT) were derived according to equation (3) shown in previous section. The percentage of occurrence is computed as the ratio between the number of nights with the presence of phase fluctuation and the total nights of observation before and during the SSW events. It is noted that 100% and 84% of the nights showed the presence of phase
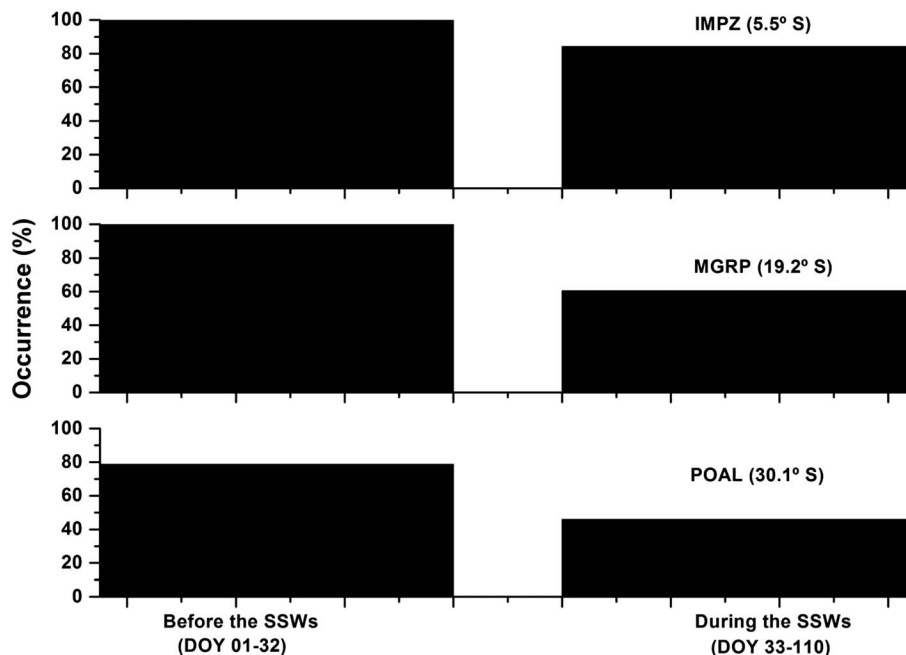
Figure 7. Percentage of nights with phase fluctuations observed during DOY 01 to 110.
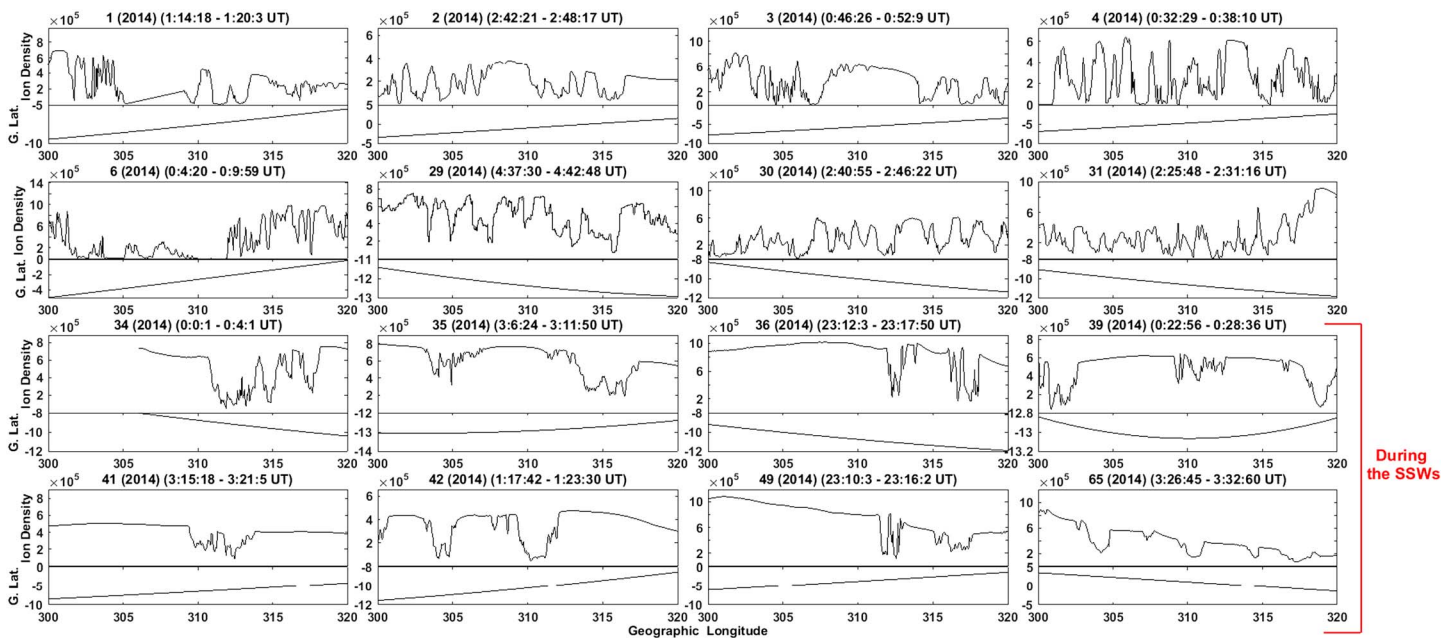
Figure 8. Time variations of the ion density measured by C/NOFS satellite from DOY 01 to DOY 65.

fluctuations at an equatorial station IMPZ before and during the SSW events, respectively. Figure 7 also reveals that 100% and 60% of the nights showed the occurrence of phase fluctuations on DOY 01–32 and DOY 33–110, respectively, at a low-latitude station MGRP. It is also observed that 79% and 46% of the nights showed the presence of phase fluctuations at another low-latitude station POAL before and during the SSW events, respectively.

Figure 8 shows the C/NOFS satellite measurements (ion density) during DOY 01 to 65. Before the 2014 SSW events, the C/NOFS satellite plot (see Figure 8) shows depletions, in the South American sector, between about 312° to 315°E (in the near vicinity of the GPS ground stations) on DOY 01 (01:14–01:20 UT), 02 (02:42–02:48 UT), 03 (00:46–00:52 UT), 04 (00:32–00:38 UT), 06 (00:04–00:09 UT), 29 (04:37–04:42 UT), 30 (02:40–02:46 UT), and 31 (02:25–02:31 UT). According to Basu et al. (2005), the ion density depletion indicates the occurrence of equatorial ionospheric irregularities. During the SSW events, Figure 8 shows that ion density depletions were present between about 312° to 315°E on DOY 34 (00:00–00:04 UT), 35 (03:06–03:11 UT), 36 (23:12–23:17 UT), 39 (00:22–00:28 UT), 41 (03:15–03:21 UT), 42 (01:17–01:23 UT), 49 (23:10–23:16 UT), and 65 (03:26–03:32 UT). However, it must be mentioned here that the ion density data were not available during DOY 76 to 110 (SSW days). The lack of the observational data (ion density) during the SSWs makes it difficult to detect the ionospheric response to the SSWs. Considering only the available data, the signature of the equatorial ionospheric irregularities in the case of Figure 8 is detected by C/NOFS satellite before and during the 2014 SSW events.

Over the magnetic equator, a strong upward $E \times B$ drift during the postsunset period is responsible for creating favorable ionospheric conditions for the formation of equatorial ionospheric irregularities, via the gravitational Rayleigh-Taylor instability (Dabas et al., 2007; Kelley, 1989). The equatorial ionospheric irregularities extend via the geomagnetic field lines to low-latitude ionosphere, and consequently, it is detectable by the ionospheric sounders at equatorial and low-latitude regions (Whalen, 2002). Several investigations (e.g., Sahai, Fagundes, & Bittencourt, 2000; Whalen, 2002, and references therein) have reported that the equatorial ionospheric irregularities exhibit large variability with day-to-day, season, and solar activities. Sahai et al. (2000) examined the seasonal variation of the ionospheric irregularities over the Brazilian sector using the OI 630 nm all-sky imaging system during high and low solar activities. Their results showed that the occurrence of the ionospheric irregularity is very low during the period of May to August, whereas it maximizes during the period of October to March. de Jesus et al. (2017) have reported that the 2012 minor SSW event affected the ionospheric irregularities in the Brazilian sector. De Paula et al. (2015) have investigated the GPS L band amplitude scintillation occurrence at a low-latitude station [São José dos Campos (23.2°S,

45.9°W; dip latitude 17.3°S)] in the Brazilian sector during 2001–2002, 2002–2003, and 2012–2013 SSW events. De Paula et al. (2015) have reported that the scintillation activity (represented by the S_4 index), during the SSW events, showed to be weaker at São José dos Campos, compared to the pre-SSW periods. Similar behavior was observed in the present investigation at IMPZ (equatorial station), MGRP, and POAL (low-latitude stations). Figure 7 shows that the phase fluctuation occurrence during the SSW events is 16% and 37% less frequent when compared with previous days (before the SSWs) at equatorial and low-latitude regions, respectively. According to Rishbeth (1971) and Eccles (1998), the zonal neutral wind in the F layer is the source of the evening prereversal enhancement (EPE). Laskar and Pallamraju (2014) reported favorable conditions for an equatorward meridional wind during the SSW events. An equatorward meridional wind can induce a decrease in the zonal neutral wind, and thus cause changes in the development of the EPE and ionospheric irregularity, during the SSW days.

4. Conclusions

The ionospheric F layer observations at the equatorial and low-latitude regions over Brazilian sector during the 2014 SSW events are investigated using GPS stations, magnetometer measurements, and C/NOFS satellite data. The main findings of this work are the following:

1. The novel aspect of the present study is that the VTEC observations over equatorial and low latitudes showed a strong increase of about 23% and 11%, respectively, around 15–22 UT during the SSW events when compared with undisturbed days (taken before the SSWs). The nighttime VTEC (0–5 UT) increased for about 8% and 33% over equatorial and low-latitude regions, respectively, during the SSW events.
2. After the second SSW temperature peak (on DOY 51), the EEJ variations showed a strong CEJ around 14–20 UT. The EEJ during the daytime (around 14–20 UT) is reduced by about 87% after the second SSW peak when compared with the previous days (before the SSWs).
3. The results from continuous wavelet transforms (CWTs) of hourly averaged VTEC and EEJ showed an amplification of oscillations with periods of 0.5 day and ~2–16 days during the 2014 SSW events. This amplification is more pronounced in semidiurnal periodicities in VTEC at equatorial and low-latitude regions.
4. The occurrences of phase fluctuations (ionospheric irregularities) are 84% and 53% in the equatorial and low-latitude regions, respectively, during the SSW periods, which is less frequent when compared to those before the SSW (100% at equatorial and 89% over at low latitudes).

References

Aarons, J., Lin, B., Mendillo, M., Liou, K., & Codrescu, M. (2000). Global Positioning System phase fluctuations and ultraviolet images from the Polar satellite. *Journal of Geophysical Research*, *105*(A3), 5201–5213. https://doi.org/10.1029/1999JA900409

Aarons, J., Mendillo, M., & Yantosca, R. (1996). GPS phase fluctuations in the equatorial region during the MISETA 1994 campaign. *Journal of Geophysical Research*, *101*(A12), 26,851–26,862. https://doi.org/10.1029/96JA00981

Aarons, J., Mendillo, M., & Yantosca, R. (1997). GPS phase fluctuations in the equatorial region during sunspot minimum. *Radio Science*, *32*(4), 1535–1550. https://doi.org/10.1029/97RS00664

Anderson, D., & Araujo-Pradere, E. A. (2010). Sudden stratospheric warming event signatures in daytime $E \times B$ drift velocities in the Peruvian and Philippine longitude sectors for January 2003 and 2004. *Journal of Geophysical Research*, *115*, A00G05. https://doi.org/10.1029/2010JA015337

Aveiro, H. C., Hysell, D. L., Caton, R. G., Groves, K. M., Klenzing, J., Pfaff, R. F., … Heelis, R. A. (2012). Three-dimensional numerical simulations of equatorial spread F: Results and observations in the Pacific sector. *Journal of Geophysical Research*, *117*, A03325. https://doi.org/10.1029/2011JA017077

Basu, S., Basu, S., Groves, K. M., MacKenzie, E., Keskinen, M. J., & Rich, F. J. (2005). Near-simultaneous plasma structuring in the midlatitude and equatorial ionosphere during magnetic superstorms. *Geophysical Research Letters*, *32*, L12S05. https://doi.org/10.1029/2004GL021678

Bessarab, F. S., Korenkov, Y. N., Klimenko, M. V., Klimenko, V. V., Karpov, I. V., Ratovsky, K. G., & Chernigovskaya, M. A. (2012). Modeling the effect of sudden stratospheric warming within the thermosphere–ionosphere system. *Journal of Atmospheric and Solar - Terrestrial Physics*, *90-91*, 77–85. https://doi.org/10.1016/j.jastp.2012.09.005

Bilitza, D., Brown, S. A., Wang, M. Y., Souza, J. R., & Roddy, P. A. (2012). Measurements and IRI model predictions during the recent solar minimum. *Journal of Atmospheric and Solar - Terrestrial Physics*, *86*, 99–106. https://doi.org/10.1016/j.jastp.2012.06.010

Burke, W. J., de La Beaujardière, O., Gentile, L. C., Hunton, D. E., Pfaff, R. F., Roddy, P. A., … Wilson, G. R. (2009). C/NOFS observations of plasma density and electric field irregularities at post-midnight local times. *Geophysical Research Letters*, *36*. L00C09. https://doi.org/10.1029/2009GL038879

Chakraborty, S. K., & Hajra, R. (2008). Solar control of ambient ionization of the ionosphere near the crest of the equatorial anomaly in the Indian zone. *Annales de Geophysique*, *26*(1), 47–57. https://doi.org/10.5194/angeo-26-47-2008

Chau, J. L., Aponte, N. A., Cabassa, E., Sulzer, M. P., Goncharenko, L. P., & González, S. A. (2010). Quiet time ionospheric variability over Arecibo during sudden stratospheric warming events. *Journal of Geophysical Research*, *115*, A00G06. https://doi.org/10.1029/2010JA015378

Chau, J. L., Fejer, B. G., & Goncharenko, L. P. (2009). Quiet variability of equatorial $E \times B$ drifts during a sudden stratospheric warming event. *Geophysical Research Letters*, *36*, L05101. https://doi.org/10.1029/2008GL036785

Chau, J. L., Goncharenko, L. P., Fejer, B. G., & Liu, H.-L. (2012). Equatorial and low latitude ionospheric effects during sudden stratospheric warming events. *Space Science Reviews*, *168*(1-4), 385–417. https://doi.org/10.1007/s11214-011-9797-5

Coster, A., Goncharenko, L., & Valladares C (2011). Longitudinal signatures in global electron total content associated with stratospheric warmings. IEEE. https://doi.org/10.1109/URSIGASS.2011.6050930

Dabas, R. S., Das, R. M., Sharma, K., Garg, S. C., Devasia, C. V., Subbarao, K. S. V., … Rao, P. V. S. R. (2007). Equatorial and low latitude spread-*F* irregularity characteristics over the Indian region and their prediction possibilities. *Journal of Atmospheric and Solar - Terrestrial Physics*, *69*(6), 685–696. https://doi.org/10.1016/j.jastp.2007.01.002

de Jesus, R., Batista, I. S., de Abreu, A. J., Fagundes, P. R., Venkatesh, K., & Denardini, C. M. (2017). Observed effects in the equatorial and low-latitude ionosphere in the South American and African sectors during the 2012 minor sudden stratospheric warming. *Journal of Atmospheric and Solar - Terrestrial Physics*, *157–158*, 78–89.

de Jesus, R., Batista, I. S., Fagundes, P. R., Venkatesh, K., & de Abreu, A. J. (2017). Ionospheric response to the 2006 sudden stratospheric warming event over the equatorial and low latitudes in the Brazilian sector using GPS observations. *Journal of Atmospheric and Solar - Terrestrial Physics*, *154*, 92–103. https://doi.org/10.1016/j.jastp.2016.12.005

De la Beaujardière, O., Jeong, L., Basu, B., Basu, S., Beach, T., Bernhardt, P., … Valladares, C. (2004). C/NOFS: A mission to forecast scintillations. *Journal of Atmospheric and Solar - Terrestrial Physics*, *66*(17), 1573–1591. https://doi.org/10.1016/j.jastp.2004.07.030

De Paula, E. R., Jonah, O. F., Moraes, A. O., Kherani, E. A., Fejer, B. G., Abdu, M. A., … Paes, R. R. (2015). Low-latitude scintillation weakening during sudden stratospheric warming events. *Journal of Geophysical Research: Space Physics*, *120*, 2212–2221. https://doi.org/10.1002/2014JA020731

Denardini, C. M., Abdu, M. A., Aveiro, H. C., Resende, L. C. A., Almeida, P. D. S. C., Olivio, E. P. A., … Wrasse, C. M. (2009). Counter electrojet features in the Brazilian sector: Simultaneous observation by radar, digital sounder and magnetometers. *Annales de Geophysique*, *27*(4), 1593–1603. https://doi.org/10.5194/angeo-27-1593-2009

Eccles, V. (1998). Modeling investigation of the evening pre-reversal enhancement of the zonal electric field in the equatorial ionosphere. *Journal of Geophysical Research*, *103*(A11), 26,709–26,719. https://doi.org/10.1029/98JA02656

Fagundes, P. R., Goncharenko, L. P., de Abreu, A. J., Venkatesh, K., Pezzopane, M., de Jesus, R., … Pillat, V. G. (2015). Ionospheric response to the 2009 sudden stratospheric warming over the equatorial, low, and middle latitudes in the South American sector. *Journal of Geophysical Research: Space Physics*, *120*, 7889–7902. https://doi.org/10.1002/2014JA020649

Fang, T.-W., Fuller-Rowell, T., Akmaev, R., Wu, F., Wang, H., & Anderson, D. (2012). Longitudinal variation of ionospheric vertical drifts during the 2009 sudden stratospheric warming. *Journal of Geophysical Research*, *117*(A3), A03324. https://doi.org/10.1029/2011JA017348

Fang, T.-W., Fuller-Rowell, T., Wang, H., Akmaev, R., & Wu, F. (2014). Ionospheric response to sudden stratospheric warming events at low and high solar activity. *Journal of Geophysical Research: Space Physics*, *119*, 7858–7869. https://doi.org/10.1002/2014JA020142

Fedrizzi, M., de Paula, E. R., Kantor, I. J., Langley, R. B., Santos, M. C., & Komjathy, A. (2002). Mapping the low-latitude ionosphere with GPS. *GPS World*, *13*(2), 41–46.

Fejer, B. G., Farley, D. T., Woodman, R. F., & Calderon, C. (1979). Dependence of equatorial *F*-region vertical drifts on season and solar-cycle. *Journal of Geophysical Research*, *84*(A10), 5792–5796. https://doi.org/10.1029/JA084iA10p05792

Fejer, B. G., Olson, M. E., Chau, J. L., Stolle, C., Lühr, H., Goncharenko, L. P., … Nagatsuma, T. (2010). Lunar dependent equatorial ionospheric electrodynamic effects during sudden stratospheric warmings. *Journal of Geophysical Research*, *115*, A00G03. https://doi.org/10.1029/2010JA015273

Fejer, B. G., Tracy, B. D., Olson, M. E., & Chau, J. L. (2011). Enhanced lunar semidiurnal equatorial vertical plasma drifts during sudden stratospheric warmings. *Geophysical Research Letters*, *38*, L21104. https://doi.org/10.1029/2011GL049788

Goncharenko, L. P., Chau, J. L., Liu, H.-L., & Coster, A. J. (2010). Unexpected connections between the stratosphere and ionosphere. *Geophysical Research Letters*, *37*, L10101. https://doi.org/10.1029/2010GL043125

Goncharenko, L. P., Coster, A. J., Chau, J. L., & Valladares, C. E. (2010). Impact of sudden stratospheric warmings on equatorial ionization anomaly. *Journal of Geophysical Research*, *115*, A00G07. https://doi.org/10.1029/2010JA015400

Grinsted, A., Moore, J. C., & Jevrejeva, S. (2004). Application of the cross wavelet transform and wavelet coherence to geophysical time series. *Nonlinear Processes in Geophysics*, *11*(5/6), 561–566. https://doi.org/10.5194/npg-11-561-2004

Hajra, R., Chakraborty, S. K., & Paul, A. (2009). Electrodynamical control of the ambient ionization near the equatorial anomaly crest in the Indian zone during counter electrojet days. *Radio Science*, *44*, RS3009. https://doi.org/10.1029/2008RS003904

Jonah, O. F., de Paula, E. R., Kherani, E. A., Dutra, S. L. G., & Paes, R. R. (2014). Atmospheric and ionospheric response to sudden stratospheric warming of January 2013. *Journal of Geophysical Research: Space Physics*, *119*, 4973–4980. https://doi.org/10.1002/2013JA019491

Joseph, O. O., Yamazak, Y., Cilliers, P., Baki, P., Ngwira, C. M., & Mito, C. (2015). A study on the response of the equatorial ionization anomaly over the East Africa sector during the geomagnetic storm of November 13, 2012. *Advances in Space Research*, *55*(12), 2863–2872. https://doi.org/10.1016/j.asr.2015.03.011

Kelley, M. C. (1989). *The Earth's ionosphere. International Geophysical Series* (Vol. 43). San Diego, CA: Academic Press.

Labitzke, K. (1981). Stratospheric-mesospheric midwinter disturbances: A summary of observed characteristics. *Journal of Geophysical Research*, *86*(C10), 9665–9678. https://doi.org/10.1029/JC086iC10p09665

Laskar, F. I., & Pallamraju, D. (2014). Does sudden stratospheric warming induce meridional circulation in the mesosphere thermosphere system? *Journal of Geophysical Research: Space Physics*, *119*, 10,133–10,143. https://doi.org/10.1002/2014JA020086

Laskar, F. I., Pallamraju, D., Lakshmi, T. V., Reddy, M. A., Pathan, B. M., & Chakrabarti, S. (2013). Investigations on vertical coupling of atmospheric regions using combined multiwavelength optical dayglow, magnetic, and radio measurements. *Journal of Geophysical Research: Space Physics*, *118*, 4618–4627. https://doi.org/10.1002/jgra.50426

Laskar, F. I., Pallamraju, D., & Veenadhari, B. (2014). Vertical coupling of atmospheres: Dependence on strength of sudden stratospheric warming and solar activity. *Earth, Planets and Space*, *66*(1), 94. https://doi.org/10.1186/1880-5981-66-94

Liu, H., Yamamoto, M., Ram, S. T., Tsugawa, T., Otsuka, Y., Stolle, C., … Nagatsuma, T. (2011). Equatorial electrodynamics and neutral background in the Asian sector during the 2009 stratospheric sudden warming. *Journal of Geophysical Research*, *116*, A08308. https://doi.org/10.1029/2011JA016607

Mannucci, A. J., Wilson, B. D., & Edwards, C. D. (1993). A new method for monitoring the Earth's ionospheric total electron content using the GPS global network. Presented at the Proceedings of ION GPS-93 (pp. 1323–1332). Salt Lake City, Utah: Institute of Navigation.

Matsuno, T. (1971). A dynamical model of the stratospheric sudden warming. *Journal of the Atmospheric Sciences*, *28*(8), 1479–1494. https://doi.org/10.1175/1520-0469(1971)028%3C1479:ADMOTS%3E2.0.CO;2

McDonald, S. E., Sassi, F., & Mannucci, A. J. (2015). SAMI3/SD-WACCM-X simulations of ionospheric variability during northern winter 2009. *Space Weather*, *13*, 568–584. https://doi.org/10.1002/2015SW001223

Medvedeva, I., Medvedev, A., Ratovsky, K., Shcherbako, V. A., & Tolstikov, M. (2015). Comprehensive study of disturbances of the neutral atmosphere and ionosphere parameters over eastern Siberia during the 2013 January major sudden stratospheric warming. *Advances in Space Research*, *56*(9), 1877–1885. https://doi.org/10.1016/j.asr.2015.06.008

Nath, O., Sridharan, S., & Gadhavi, H. (2015). Equatorial stratospheric thermal structure and ozone variations during the sudden stratospheric warming of 2013. *Journal of Atmospheric and Solar - Terrestrial Physics*, *122*, 129–137. https://doi.org/10.1016/j.jastp.2014.11.003

Paes, R. R., Batista, I. S., Candido, C. M. N., Jonah, O. F., & Santos, P. C. P. (2014). Equatorial ionization anomaly variability over the Brazilian region during boreal sudden stratospheric warming events. *Journal of Geophysical Research: Space Physics*, *119*, 7649–7664. https://doi.org/10.1002/2014JA019968

Pancheva, D., & Mukhtarov, P. (2011). Stratospheric warmings: The atmosphere-ionosphere coupling paradigm. *Journal of Atmospheric and Solar - Terrestrial Physics*, *73*(13), 1697–1702. https://doi.org/10.1016/j.jastp.2011.03.066

Pedatella, N. M., & Liu, H.-L. (2013). The influence of atmospheric tide and planetary wave variability during sudden stratosphere warmings on the low latitude ionosphere. *Journal of Geophysical Research: Space Physics*, *118*, 5333–5347. https://doi.org/10.1002/jgra.50492

Pedatella, N. M., & Forbes, J. M. (2010). Evidence for stratosphere sudden warming-ionosphere coupling due to vertically propagating tides. *Geophysical Research Letters*, *37*, L11104. https://doi.org/10.1029/2010GL043560

Pedatella, N. M., Liu, H.-L., Richmond, A. D., Maute, A., & Fang, T.-W. (2012). Simulations of solar and lunar tidal variability in the mesosphere and lower thermosphere during sudden stratosphere warmings and their influence on the low-latitude ionosphere. *Journal of Geophysical Research*, *117*, A08326. https://doi.org/10.1029/2012JA017858

Rao, P. V. S. R., Krishna, S. G., Niranjan, K., & Prasad, D. S. V. V. D. (2006). Temporal and spatial variations in TEC using simultaneous measurements from the Indian GPS network of receivers during the low solar activity period of 2004–2005. *Annales de Geophysique*, *24*, 3279–3292.

Rastogi, R. G. (1999). Morphological aspects of a new type of counter electrojet event. *Annales de Geophysique*, *17*(2), 210–219. https://doi.org/10.1007/s00585-999-0210-6

Rishbeth, H. (1971). Polarization fields produced by winds in the equatorial *F* region. *Planetary and Space Science*, *19*(3), 357–369. https://doi.org/10.1016/0032-0633(71)90098-5

Sahai, Y., Fagundes, P. R., & Bittencourt, J. A. (2000). Transequatorial *F*-region ionospheric plasma bubbles: Solar cycle effects. *Journal of Atmospheric and Terrestrial Physics*, *62*(15), 1377–1383. https://doi.org/10.1016/S1364-6826(00)00179-6

Scherhag, R. (1952). Die explosion sartige Stratospharenerwärmung des Spa1951/52. *Berichte des Deutschen Wetterdienstes*, *38*, 51–63.

Shume, E. B., Denardini, C. M., De Paula, E. R., & Trivedi, N. B. (2010). Variabilities of the equatorial electrojet in Brazil and Perú. *Journal of Geophysical Research*, *115*, A06306. https://doi.org/10.1029/2009JA014984

Siddiqui, T. A., Lühr, H., Stolle, C., & Park, J. (2015). Relation between stratospheric sudden warming and the lunar effect on the equatorial electrojet based on Huancayo recordings. *Annales de Geophysique*, *33*(2), 235–243. https://doi.org/10.5194/angeo-33-235-2015

Sridharan, S., Sathishkumar, S., & Gurubaran, S. (2009). Variabilities of mesospheric tides and equatorial electrojet strength during major stratospheric warming events. *Annales de Geophysique*, *27*(11), 4125–4130. https://doi.org/10.5194/angeo-27-4125-2009

Torrence, C., & Compo, G. P. (1998). A practical guide to wavelet analysis. *Bulletin of the American Meteorological Society*, *79*(1), 61–78. https://doi.org/10.1175/1520-0477(1998)079%3C0061:APGTWA%3E2.0.CO;2

Upadhayaya, A. K., & Mahajan, K. K. (2013). Ionospheric F_2 region: Variability and sudden stratospheric warmings. *Journal of Geophysical Research: Space Physics*, *118*, 6736–6750. https://doi.org/10.1002/jgra.50570

Vieira, F., Fagundes, P. R., Venkatesh, K., Goncharenko, L. P., & Pillat, V. G. (2017). Total electron content disturbances during minor sudden stratospheric warming, over the Brazilian region: A case study during January 2012. *Journal of Geophysical Research: Space Physics*, *122*, 2119–2135. https://doi.org/10.1002/2016JA023650

Vineeth, C., Pant, T. K., & Sridharan, R. (2009). Equatorial counter electrojets and polar stratospheric sudden warmings: A classical example of high latitude-low latitude coupling? *Annales de Geophysique*, *27*(8), 3147–3153. https://doi.org/10.5194/angeo-27-3147-2009

Whalen, J. A. (2002). Dependence of equatorial bubbles and bottom side spread *F* on season, magnetic activity, and $E \times B$ drift velocity during solar maximum. *Journal of Geophysical Research*, *107*(A2), 1024. https://doi.org/10.1029/2001JA000039

Yamazaki, Y., Yumoto, K., McNamara, D., Hirooka, T., Uozumi, T., Kitamura, K., … Ikeda, A. (2012). Ionospheric current system during sudden stratospheric warming events. *Journal of Geophysical Research*, *117*, A03334. https://doi.org/10.1029/2011JA017453

Yue, X., Schreiner, W. S., Lei, J., Rocken, C., Hunt, D. C., Kuo, Y.-H., & Wan, W. (2010). Global ionospheric response observed by cosmic satellites during the January 2009 stratospheric sudden warming event. *Journal of Geophysical Research*, *115*, A00G09. https://doi.org/10.1029/2010JA015466